Drying Technology
An International Journal
Publication details, including instructions for authors and subscription information:
http://www.informaworld.com/smpp/title~content=t713597247

Analysis of Multiphase Flow and Heat Transfer: Pressure Buildup in an Unsaturated Porous Slab Exposed to Hot Gas

P. Rattanadecho [a]; W. Pakdee [a]; J. Stakulcharoen [a]
[a] Research Center of Microwave Utilization in Engineering (R.C.M.E), Department of Mechanical Engineering, Faculty of Engineering, Thammasat University, Klong Luang, Pathumthani, Thailand

Online Publication Date: 01 January 2008
To cite this Article: Rattanadecho, P., Pakdee, W. and Stakulcharoen, J. (2008) 'Analysis of Multiphase Flow and Heat Transfer: Pressure Buildup in an Unsaturated Porous Slab Exposed to Hot Gas', Drying Technology, 26:1, 39 - 53
To link to this article: DOI: 10.1080/07373930701781231
URL: http://dx.doi.org/10.1080/07373930701781231

Drying Technology, 26: 39–53, 2008

ISSN: 0737-3937 print/1532-2300 online
DOI: 10.1080/07373930701781231

Taylor & Francis
Taylor & Francis Group

Analysis of Multiphase Flow and Heat Transfer: Pressure Buildup in an Unsaturated Porous Slab Exposed to Hot Gas

P. Rattanadecho, W. Pakdee, and J. Stakulcharoen

Research Center of Microwave Utilization in Engineering (R.C.M.E), Department of Mechanical Engineering, Faculty of Engineering, Thammasat University, Klong Luang, Pathumthani, Thailand

This study develops a mathematical model for coupled heat and mass transfer in an unsaturated porous slab exposed to a flowing hot gas. Effects of the initial saturation conditions on associated variables, i.e., total pressure, temperature, moisture content, and multiphase flow, are studied. The Newton-Raphson method based on a finite volume technique is applied. This study emphasizes the influence of initial saturation level and gravitational effect in heat and multiphase flow phenomena associated with this system. Gravity enhances the downward flow of liquid within the porous slab. Pressure buildup occurs near the interface between the wet and the dry zone. However, it appears that the order of magnitude to the total pressure is small. This study explains the fundamental mechanism of multiphase flow that involves heat and mass transfer in a heated unsaturated porous slab.

Keywords Concrete; Drying; Heat and mass transfer; Numerical method; Porous medium

INTRODUCTION

The study of heated porous slab behaviors is important for assessment of fire safety in buildings. Heat and mass transfer in porous materials have been carried out both theoretically and empirically.[1,2] Many theories regarding the physical phenomena of heat and mass transfer in porous materials have been proposed in the literature; e.g., the diffusion theory, the capillary flow theory, the evaporation-condensation theory, etc. The popular drying theory proposed by Whitaker[3] and Patankar[4] is very well known. This theory is based on volume-averaged conservation equations for a two-phase capillary flow in porous media. The mathematical models for simultaneous heat and mass transfer during heating of porous media were studied extensively by Boukadida et al.[5] and Perre et al.[6] Most models are based on Whitaker's theory and are focused on heat and mass transfer as well as the total pressure. Ratanadecho et al.[7–9] conducted their study on the drying process of a multilayered porous packed bed using microwave energy. In their experimental and theoretical study of the development of high-temperature convective drying, Perre et al.[10] investigated two drying fluids: moist air and superheated steam. Two materials, light concrete and softwood, were used. Ben Nasrallah et al.[11] studied the model of heat and mass transfer in porous media deduced from Whitaker's theory. Their model comprised a very comprehensive set of equations. In addition, the gaseous pressure was also concluded. Their system of equations with unidirectional transfers was numerically solved. Chen et al.[12] studied the model of heat and mass transfer in porous media in which the concept of bound water conductivity was introduced. It was found that the bound water conductivity was affected by moisture content as well as desorption isotherms of the drying materials. Also, the major internal moisture transfer mechanisms are considered to be capillary flow of the water in the wet regions, and movements of bound water and vapor transfer in the sorption region.

The study of Wei et al.[13] developed a mathematical model to predict the heat and mass transfer phenomena in porous materials. Their model also predicted the fluid flow pattern in the heated samples. They modified Whitaker's derivations and applied the new model to sandstone subjected to mild heating conditions. Boukadida et al.[14] studied two-dimensional heat and mass transfer during a convective drying of porous media. The effect of internal total pressure was taken into account in the set of macroscopic equations. Gaseous diffusion was generated as the gradient of vapor pressure. Darcy's law was used in their model.

The model describing the drying of a slab of porous material in a combined microwave and convective environment has been formulated by the study of Turner et al.[15] The inclusion of pressure in the model allows the physical

Correspondence: P. Rattanadecho, Research Center of Microwave Utilization in Engineering (R.C.M.E), Department of Mechanical Engineering, Faculty of Engineering, Thammasat University, Rangsit Campus, 99 Mu 18, Klong Luang, Pathumthani 12120, Thailand; E-mail: ratphadu@engr.tu.ac.th

phenomena of "water pumping" to be accounted for. During the drying process, the sample size played an important role in the drying kinetics. In particular, the effect of resonance on the moisture, temperature profiles, and surface mass transfer coefficients were investigated.

Huang et al.[16,17] conducted their study, focusing on the hygrothermal behavior of concrete slabs with external conditions very closed to those of the atmospheric surroundings. The developed theory is applied to the investigation of moisture migration in the light-weight subject to a temperature gradient. In their study, the coupled heat and mass transfer in concrete structures at high temperatures being contributed by fire was simulated. The numerical results were used to predict the phenomenon of *moisture clog* and the explosive spalling of concrete under fire. It showed that the sealed layer as a fire protection had significant effects on the buildup pore pressure in the concrete walls, which, in turn, improved the susceptibility of fire damage. The assumptions on the porous system and the transport process found were multiphase, solid, rigid, and incompressible liquid. However, mobility of liquid was assumed to be negligible and fluid movement was not studied in details. Extensive attention has given to interesting investigations on drying of refractory concrete including the pressure effects leading to spalling of refractories, a problem of considerable industrial interest.[19–23]

Pakdee and Rattanadecho[24] have studied numerical investigations of transient natural convection flow through a fluid-saturated porous medium in a rectangular cavity with a convection surface condition. The two-dimensional flow is mainly characterized by two symmetrical vortices driven by the effect of buoyancy. A lateral temperature gradient in the region close to the top wall induces the buoyancy force under an unstable condition. Unsteady effects of associated parameters were examined. It was found that the heat transfer coefficient, Rayleigh number, and Darcy number considerably influenced characteristics of flow and heat transfer mechanisms. Furthermore, the flow pattern was found to have a local effect on the heat convection rate. Recently, Gawin et al.[25] have studied a mathematical model of hygro-thermochemo-mechanical phenomena in heated concrete. Contribution of the stored elastic energy and vapor pressure buildup to the kinetic energy of spalled concrete pieces is estimated. Different simplified models of thermal spalling are used to define special indexes, aiming for quantitative assessment of its risk. A simplified energy analysis to estimate the kinetic energy of spalled concrete pieces and to make predictions about explosive or nonviolent character of the phenomenon is proposed.

In the present study, a mathematical model, simulating the coupled heat and mass transfer in one dimensional unsaturated porous slab exposed to hot gas, has been developed. This study emphasized the influence of initial saturations and of gravitational effect in heat and multiphases flow phenomena. The different conditions with and without gravitational force are studied. Three different initial saturations are applied. Besides, this study significantly simulates the timely combination of the magnitude and direction of fluid movements in each phase in the permeable heated porous slab at various times. This model yields a number of considerations of changes in temperature, saturation, rates of mass and heat transfer during the hot gas exposure. The three parameters are taken into account. No previous study showed the relationship between the multiphases flow phenomena and various initial saturations within the unsaturated porous slab subjected to hot gas.

GOVERNING EQUATIONS

A one dimensional unsaturated porous slab exposed to hot gas is schematically shown in Fig. 1. In this study, unsaturated porous slab is assumed to be a nonhygroscopic porous medium that is homogeneous, isotropic, and reproducible. It is basically composed of solid phase, water phase, and air phase. The porosity and permeability within unsaturated porous slab were selected as 0.16 and 1.1×10^{-12}, respectively. One surface of the wall ($z = 0$ cm) cm) is exposed to hot gas at 170°C and the other surface ($z = 20$ cm) remains under atmospheric conditions, both surfaces allow the heat and mass to transfer freely through the surface to the ambient. In this analysis, the main assumptions involved in the formulation of the transport model are

1 The capillary porous material is rigid and no chemical reactions occur in the sample.
2 Local thermodynamic equilibrium among each phase is assumed.

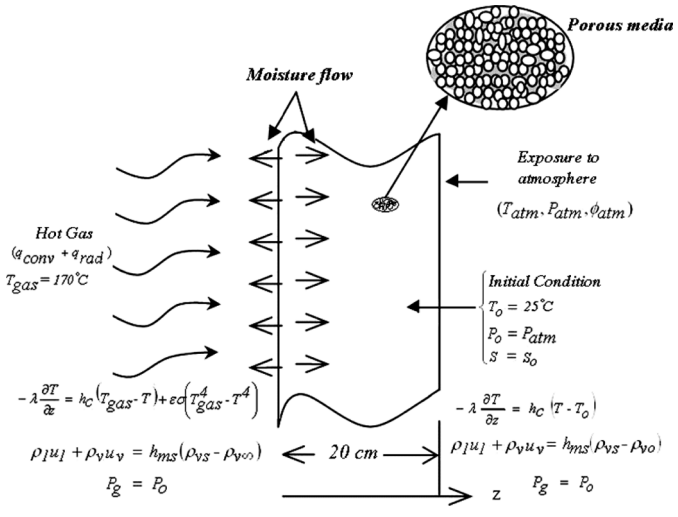

FIG. 1. Physical model of unsaturated porous slab exposed to hot gas.

3 The gas phase is ideal in the thermodynamic sense.
4 The contribution of convection to energy transport is included.
5 Darcy's law holds for the liquid and gas phases.
6 Gravity is included particularly in the liquid and gas phases.
7 Permeabilities of liquid and gas can be expressed in term of relative permeability.
8 In a macroscopic sense, the packed bed is assumed to be homogeneous and isotropic, and liquid water is not bound to the solid matrix. Therefore, the volume average model for a homogeneous and isotropic material can be used in the theoretical model and analysis.
9 A dry layer (evaporation front) is formed immediately after water saturation approaches the irreducible value.
10 This study neglects dehydration and water mass sources and heat sinks related to this phenomenon.

The physical properties and coefficient values employed in the computational work are given in Table 1.

By considering conservation of mass and energy in the unsaturated porous slab, the governing equation of mass and energy for all phases can be derived using the volume-averaging technique. The main basic equations for unsaturated porous slab are given by the following equations.

TABLE 1
Values of the physical properties

Symbol	Value	Unit
ρ_w	900	kg/m^3
C_{pw}	4386.0	J/kg K
μ_w	1.5×10^{-4}	kg/m · s
λ_w	0.68	W/m K
C_{pa}	1020	J/kg K
C_{pv}	1860	J/kg K
C_{pg}	1020	J/kg K
μ_g	2.5×10^{-5}	kg/m · s
λ_g	0.0373	W/m K
ρ_P	2300	kg/m^3
C_{pp}	800.0	J/kg K
λ_p	1.40	W/m K
D_0	2.19×10^{-5}	m^2/s
s_{ir}	0.06	—
K	1.1×10^{-12}	m^2
h_v	2.407×10^6	J/kg
h_c	15	W/m^{2}K
ε	0.9	—
T_o	25	°C
T_{gas}	170	°C

Mass Conservation Equations

The microscopic mass conservation equations for liquid, water vapor, air, and gas phases, are written, respectively, as:

$$\text{Liquid phase} \quad \frac{\partial}{\partial t}(\rho_l \phi s) + \frac{\partial}{\partial z}(\rho_l u_l) = -\dot{n} \tag{1}$$

$$\text{Vapor phase} \quad \frac{\partial}{\partial t}\{\rho_v \phi(1-s)\} + \frac{\partial}{\partial z}(\rho_v u_v) = \dot{n} \tag{2}$$

$$\text{Air phase} \quad \frac{\partial}{\partial t}\{\rho_a \phi(1-s)\} + \frac{\partial}{\partial z}(\rho_a u_a) = 0 \tag{3}$$

$$\text{Gas phase} \quad \frac{\partial}{\partial t}\{\rho_g \phi(1-s)\} + \frac{\partial}{\partial z}(\rho_g u_g) = \dot{n} \tag{4}$$

where $\dot{n}$ is a condensation rate or an evaporation rate during phase change. The water vapor and air mass flux is the sum of the convective term with the gas superficial velocity and diffusive term.

In order to complete the system of equations, the expressions for the superficial average velocity of the liquid and gas phase the generalized Darcy's law in the following form is used:[9]

$$u_l = -\frac{KK_{rl}}{\mu_l}\left[\frac{\partial P_g}{\partial z} - \frac{\partial P_c}{\partial z} - \rho_l g\right] \tag{5}$$

$$u_g = -\frac{KK_{rg}}{\mu_g}\left[\frac{\partial P_g}{\partial z} - \rho_g g\right] \tag{6}$$

For the velocity of water vapor and air phase the generalized Fick's law for a two-component gas mixture can be expressed as:

$$\rho_v u_v = \rho_v u_g - \rho_g D_m \frac{\partial}{\partial z}\left(\frac{\rho_v}{\rho_g}\right) \tag{7}$$

$$\rho_a u_a = \rho_a u_g - \rho_g D_m \frac{\partial}{\partial z}\left(\frac{\rho_a}{\rho_g}\right) \tag{8}$$

where the capillary pressure P_c related to the gas and liquid phases can be written by:

$$P_c = P_g - P_l \tag{9}$$

D_m is the effective molecular mass diffusion:

$$D_m = \frac{2\phi}{3-\phi}(1-s)D_0 \tag{10}$$

and D_0 is binary mass diffusion in plain media:

$$D = D_0\left(\frac{p_0}{p}\right)\left(\frac{T}{T_0}\right)^{2.2} \tag{11}$$

The system of conservation equations obtained for multiphase transport mode requires constitutive equation

for relative permeabilities K_r, capillary pressure p_c, capillary pressure functions J, and effective thermal conductivity λ_{eff}. A typical set of constitutive relationships for liquid and gas system is given by:[9]

$$K_{rl} = s_e^3 \tag{12}$$

$$K_{rg} = (1 - s_e)^3 \tag{13}$$

where s_e is the effective water saturation, which is considered to be the irreducible water saturation s_{ir}. The symbol S denotes water saturation that is related to the effective water saturation s_e as shown in the below equation:

$$s_e = \frac{s - s_{ir}}{1 - s_{ir}} \tag{14}$$

The capillary pressure P_c is further assumed to be adequately by Leverett's well known $J(s_e)$ functions. The relationship between the capillary pressure and the water saturation is represented by using Leverett function $J(s_e)$:[9]

$$p_c = p_g - p_l = \frac{\xi}{\sqrt{K/\phi}} J(s_e) \tag{15}$$

where ξ is the gas-liquid interfacial tension and $J(s_e)$ is defined as:

$$J(s_e) = 0.325(1/s_e - 1)^{0.217} \tag{16}$$

Moisture Equation

The phenomenon of moisture transport is described by the mass conservation equations for the liquid phase and for the water vapor in gas phase since total water content is of interest. The addition of those one dimensional equations (Eqs. (1) and (2)) yields total moisture content as follows:

$$\phi \frac{\partial}{\partial t}\{\rho_1 s + \rho_v(1 - s)\} + \frac{\partial}{\partial z}[\rho_1 u_1 + \rho_v u_v] = 0 \tag{17}$$

Pressure Equation

The total pressure is obtained from air-balance equation (Eq. (3)) as:

$$\frac{\partial}{\partial t}\{\rho_a \phi(1 - s)\} + \frac{\partial}{\partial z}[\rho_a u_a] = 0 \tag{18}$$

Energy Equation

The kinetic energy and pressure terms, which are usually unimportant are ignored. Local thermodynamics equilibrium among all phases is assumed. The temperature of unsaturated porous slab exposed to hot gas is obtained by solving the conventional heat transport equation. Considering the enthalpy transport based on the water and gas flows, the conduction heat and latent heat transfer due to evaporation. The energy conservation equation is represented by:

$$\frac{\partial}{\partial t}[(\rho C_p)_T T] + \nabla[\{\rho_l C_{pl} u_l + (\rho_a C_{pa} + \rho_v C_{pv}) u_g\} T] = -\nabla q - h_{lv}\dot{n} \tag{19}$$

State Equation

Gas phase is assumed to be an ideal mixture of air and vapor, so density of each phase can be determined from the below equations:[4]

$$\begin{aligned} \rho_a &= \frac{P_a M_a}{R_o T} \\ \rho_v &= \frac{P_v M_v}{R_o T} \\ \rho_g &= \rho_a + \rho_v \\ P_a &= \rho_a R_a T \\ P_v &= \rho_v R_v T \\ \rho_g u_g &= \rho_a u_g + \rho_v u_v \end{aligned} \tag{20}$$

The partial pressure of the vapor is given by Kelvin's equation based on the capillary force defined by:

$$P_v = P_{vs} \exp\left(\frac{P_c}{\rho_l R_v T}\right) \tag{21}$$

where the p_{vs} is the partial pressure of the saturation vapor.

Substitution of Eqs. (5)–(7) into Eq. (17) results in a moisture equation as:

$$\phi \frac{\partial}{\partial t}\{\rho_l s + \rho_v(1 - s)\} + \frac{\partial}{\partial z}\left[\rho_l \frac{KK_{rl}}{\mu_l}\left(\frac{\partial P_c}{\partial z} - \frac{\partial P_g}{\partial z} + \rho_l g\right) + \rho_v \frac{KK_{rg}}{\mu_g}\left(-\frac{\partial P_g}{\partial z} + \rho_g g\right) - \rho_g D_m \frac{\partial}{\partial z}\left(\frac{\rho_v}{\rho_g}\right)\right] = 0 \tag{22}$$

with the application of Darcy's law (Eq. (6)) and Fick's law (Eq. (8)), the total pressure equation (Eq. (18)) is written as:

$$\phi \frac{\partial}{\partial t}\{\rho_a(1 - s)\} + \frac{\partial}{\partial z}\left[\rho_a \frac{KK_{rg}}{\mu_g}\left(-\frac{\partial P_g}{\partial z} + \rho_g g\right) - \rho_g D_m \frac{\partial}{\partial z}\left(\frac{\rho_a}{\rho_g}\right)\right] = 0 \tag{23}$$

Also, the energy equation (Eq. (19)) can be expressed as:

$$\frac{\partial}{\partial t}\left\{(\rho c_p)_T T\right\} + \frac{\partial}{\partial z}\left[\left\{\rho_l c_{pl} u_l + (\rho_a c_{pa} + \rho_v c_{pv}) u_g\right\} T\right] = \frac{\partial}{\partial z}\left[\lambda \frac{\partial T}{\partial z}\right] - h_{lv}\left\{\frac{\partial}{\partial t}\{\rho_v \phi(1-s)\} + \frac{\partial}{\partial z}\left[\rho_v \frac{KK_{rg}}{\mu_g}\left(-\frac{\partial P_g}{\partial z} + \rho_g g\right) - \rho_g D_m \frac{\partial}{\partial z}\left(\frac{\rho_v}{\rho_g}\right)\right]\right\} \quad (24)$$

Boundary Conditions and Initial Condition

With corresponding to Fig. 1, two boundary conditions, at the permeable heated surface and the permeable unheated surface are formulated. The analysis of each condition is shown. *Permeable Heating Surface* ($z = 0$ cm). cm). The boundary conditions proposed for the permeable heating surface, convection, and radiation take place at its boundary, which is subsequently transferred to medium by conduction. The equation can be described as follows:

$$-\lambda \frac{\partial T}{\partial z} = h_c(T_{gas} - T) + \varepsilon\sigma(T_{gas}^4 - T^4) \quad (25)$$

where the mass transfer at the permeable surface is modeled by means of a local constant mass transfer coefficient, which is related to the local water vapor flux density:

$$\rho_1 u_1 + \rho_v u_v = h_{ms}(\rho_{vs} - \rho_{v\infty}) \quad (26)$$

where the mass transfer coefficient, h_{ms}, at the permeable surfaces depend on the surface saturation coefficient which varies with average water saturation. The total pressure at the permeable surface can be defined as:

$$P_g = P_o \quad (27)$$

where P_o is atmospheric pressure.

Permeable Unheated Surface ($z = 20$ cm). For the permeable unheated surface, only convection takes place at its boundary which is subsequently transferred from medium to ambient by conduction. The equation is then given by:

$$-\lambda \frac{\partial T}{\partial z} = h_c(T - T_o) \quad (28)$$

The boundary equations for mass transfer and for total pressure are the same as ones for the heated surface.

The initial conditions used in this study are

$$P_o = P_{atm}, \quad T_o = 25^\circ C, \quad S = S_o \quad (29)$$

Furthermore, in case of without gravitational force, the above equations can also be applied, by neglecting the terms involving the gravitational force.

NUMERICAL METHOD

In this study, the coupled nonlinear set of energy and of mass equations with regard to water saturation, total gas pressure and temperature were numerically solved by a method of finite differences based on the notion of control domain as described by Patankar.[4] The method has an advantage of ensuring flux conservation; the generations of parasitic sources are thus avoided. The basic strategy of finite control volume discretization technique is to divide the calculated domain into a number of control volumes.[14] At the boundaries of the calculated domain, the equations were discretized by integrating over half the control volume and by taking into account the boundary conditions. At the corners of the calculated domain we use a quarter of control volume. Then, the conservation equations are integrated over this control volume and interval of time. The method creates nodal values of moisture content, total pressure, and temperature, which are solved iteratively. The Newton-Raphson method was employed at each iteration to improve the convergence rate. The discretized form of moisture equation (Eq. (22)) is given by:

$$\frac{\phi}{\Delta t}\left\{\rho_l(1-s_{ir})(s_{ek}^{n+1} - s_{ek}^n) + (1-s_{ir})(\rho_{vk}^{n+1}(1-s_{ek}^{n+1}) - \rho_{vk}^n(1-s_{ek}^n))\right\} + \frac{1}{\Delta z}\left\{\begin{array}{l} \rho_l\left[\left.\frac{KK_{rl}}{\mu_l}\right|_{k+\frac{1}{2}}\left(\left(\frac{P_{ck+1}^{n+1} - P_{ck}^{n+1}}{\Delta z}\right) - \left(\frac{P_{gk+1}^{n+1} - P_{gk}^{n+1}}{\Delta z}\right) + \rho_l g\right)\right. \\ \left. - \left.\frac{KK_{rl}}{\mu_l}\right|_{k-\frac{1}{2}}\left(\left(\frac{P_{ck}^{n+1} - P_{ck-1}^{n+1}}{\Delta z}\right) - \left(\frac{P_{gk}^{n+1} - P_{gk-1}^{n+1}}{\Delta z}\right) + \rho_l g\right)\right] \\ + \left[\rho_{vk}^{n+1}\left.\frac{KK_{rg}}{\mu_g}\right|_{k+\frac{1}{2}}\left(-\left(\frac{P_{gk+1}^{n+1} - P_{gk}^{n+1}}{\Delta z}\right) + \rho_{gk}^{n+1} g\right)\right. \\ \left. - \rho_{vk-1}^{n+1}\left.\frac{KK_{rg}}{\mu_g}\right|_{k-\frac{1}{2}}\left(-\left(\frac{P_{gk}^{n+1} - P_{gk-1}^{n+1}}{\Delta z}\right) + \rho_{gk-1}^{n+1} g\right)\right] \\ - \left[\rho_{gk}^{n+1} D_{mk+\frac{1}{2}}^{n+1}\left(\frac{\left(\frac{\rho_v}{\rho_g}\right)_{k+1}^{n+1} - \left(\frac{\rho_v}{\rho_g}\right)_k^{n+1}}{\Delta z}\right)\right. \\ \left. - \rho_{gk-1}^{n+1} D_{mk-\frac{1}{2}}^{n+1}\left(\frac{\left(\frac{\rho_v}{\rho_g}\right)_k^{n+1} - \left(\frac{\rho_v}{\rho_g}\right)_{k-1}^{n+1}}{\Delta z}\right)\right] \end{array}\right\} = 0 \quad (30)$$

Similarly, the discretized form of total pressure equation (Eq. (23)) can be written as:

$$\frac{\phi}{\Delta t}\left\{(1-s_{ir})(\rho_{ak}^{n+1}(1-s_{ek}^{n+1})-\rho_{ak}^{n}(1-s_{ek}^{n}))\right\}$$
$$+\frac{1}{\Delta z}\left\{\begin{array}{l}\left[\rho_{ak}^{n+1}\left.\frac{KK_{rg}}{\mu_g}\right|_{k+\frac{1}{2}}\left(-\left(\frac{P_{gk+1}^{n+1}-P_{gk}^{n+1}}{\Delta z}\right)+\rho_{gk}^{n+1}g\right)\right.\\ \left.-\rho_{ak-1}^{n+1}\left.\frac{KK_{rg}}{\mu_g}\right|_{k-\frac{1}{2}}\left(-\left(\frac{P_{gk}^{n+1}-P_{gk-1}^{n+1}}{\Delta z}\right)+\rho_{gk-1}^{n+1}g\right)\right]\\ -\left[\rho_{gk}^{n+1}D_{mk+\frac{1}{2}}^{n+1}\left(\frac{\left(\frac{\rho_a}{\rho_g}\right)_{k+1}^{n+1}-\left(\frac{\rho_a}{\rho_g}\right)_{k}^{n+1}}{\Delta z}\right)\right.\\ \left.-\rho_{gk-1}^{n+1}D_{mk-\frac{1}{2}}^{n+1}\left(\frac{\left(\frac{\rho_a}{\rho_g}\right)_{k}^{n+1}-\left(\frac{\rho_a}{\rho_g}\right)_{k-1}^{n+1}}{\Delta z}\right)\right]\end{array}\right\}$$
$$=0 \tag{31}$$

The discretized form of energy equation (Eq. (24)) can also be written as

$$\frac{(\rho C_p)_{Tk}^{n+1}T_k^{n+1}-(\rho C_p)_{Tk}^{n}T_k^{n}}{\Delta t}+\frac{\rho_l C_{pl}}{\Delta z}\left(u_{lk}^{n+1}T_k^{n+1}-u_{lk-1}^{n+1}T_{k-1}^{n+1}\right)$$
$$+\frac{(\rho C_p)_{av}}{\Delta z}\left(u_{gk}^{n+1}T_k^{n+1}-u_{gk-1}^{n+1}T_{k-1}^{n+1}\right)$$
$$-\frac{1}{\Delta z}\left[\lambda_{k+\frac{1}{2}}^{n+1}\left(\frac{T_{k+1}^{n+1}-T_k^{n+1}}{\Delta z}\right)-\lambda_{k-\frac{1}{2}}^{n+1}\left(\frac{T_k^{n+1}-T_{k-1}^{n+1}}{\Delta z}\right)\right]$$
$$+\frac{h_{lv}\rho_v\phi}{\Delta t}\left\{(1-s_{ir})(s_{ek}^{n+1}-s_{ek}^{n})\right\}$$
$$+\frac{1}{\Delta z}\left\{\begin{array}{l}\left(\rho_{vk}^{n+1}\left.\frac{KK_{rg}}{\mu_g}\right|_{k+\frac{1}{2}}\left(-\left(\frac{P_{gk+1}^{n+1}-P_{gk}^{n+1}}{\Delta z}\right)+\rho_{gk}^{n+1}g\right)\right.\\ \left.-\rho_{vk-1}^{n+1}\left.\frac{KK_{rg}}{\mu_g}\right|_{k-\frac{1}{2}}\left(-\left(\frac{P_{gk}^{n+1}-P_{gk-1}^{n+1}}{\Delta z}\right)+\rho_{gk-1}^{n+1}g\right)\right)\\ -\left(\begin{array}{l}\rho_{gk}^{n+1}D_{mk+\frac{1}{2}}^{n+1}\left(\frac{\left(\frac{\rho_v}{\rho_g}\right)_{k+1}^{n+1}-\left(\frac{\rho_v}{\rho_g}\right)_{k}^{n+1}}{\Delta z}\right)\\ -\rho_{gk-1}^{n+1}D_{mk-\frac{1}{2}}^{n+1}\left(\frac{\left(\frac{\rho_v}{\rho_g}\right)_{k}^{n+1}-\left(\frac{\rho_v}{\rho_g}\right)_{k-1}^{n+1}}{\Delta z}\right)\end{array}\right)\end{array}\right\}$$
$$=0 \tag{32}$$

The coupled nonlinear set of Eqs. (30)–(32) in regard to water saturation, total pressure, and temperature were numerically solved by using the finite control volume technique as explained above. The computational schemes and strategy are detailed in Fig. 2. To attain greater precision without increasing the number of nodes in the grid during calculation, the grid will be recalculated as there are significant changes of relative slope. The values used in the computation for 100 nodes are $\Delta z = 2\times10^{-3}$ m and $\Delta t = 0.01$ s with relative error of 1.0×10^{-8}.

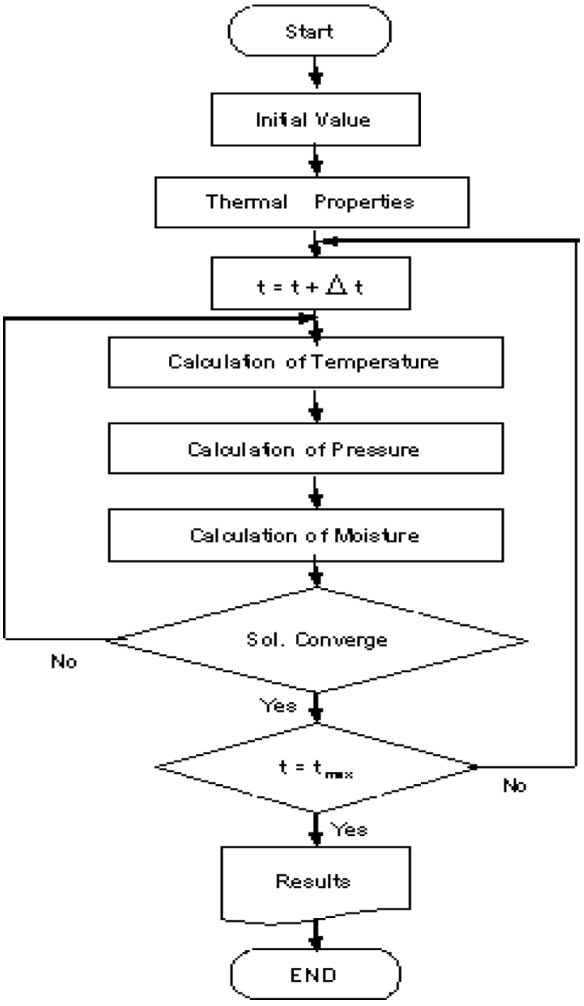

FIG. 2. Computational scheme.

To verify the accuracy of the presented numerical study, the resulting data is validated against the results obtained by Rogers and Kaviany.[26] Figure 3a shows the predicted result[26] and Fig. 3b shows the results from the presented study. Both are in good agreement. At $t = 114$ min, the study shows that the distribution curve gradually declines at unheated surface from X/L of 0.7 onwards. This suggests that the additional conditions in the present mode under the same numerical approach yields a nontrivial difference at $t = 114$ min.

RESULTS AND DISCUSSION

In one dimensional unsaturated porous slab exposed to hot gas, one surface of the wall ($z = 0$ cm) is exposed to hot gas at 170°C and the other surface ($z = 20$ cm that for

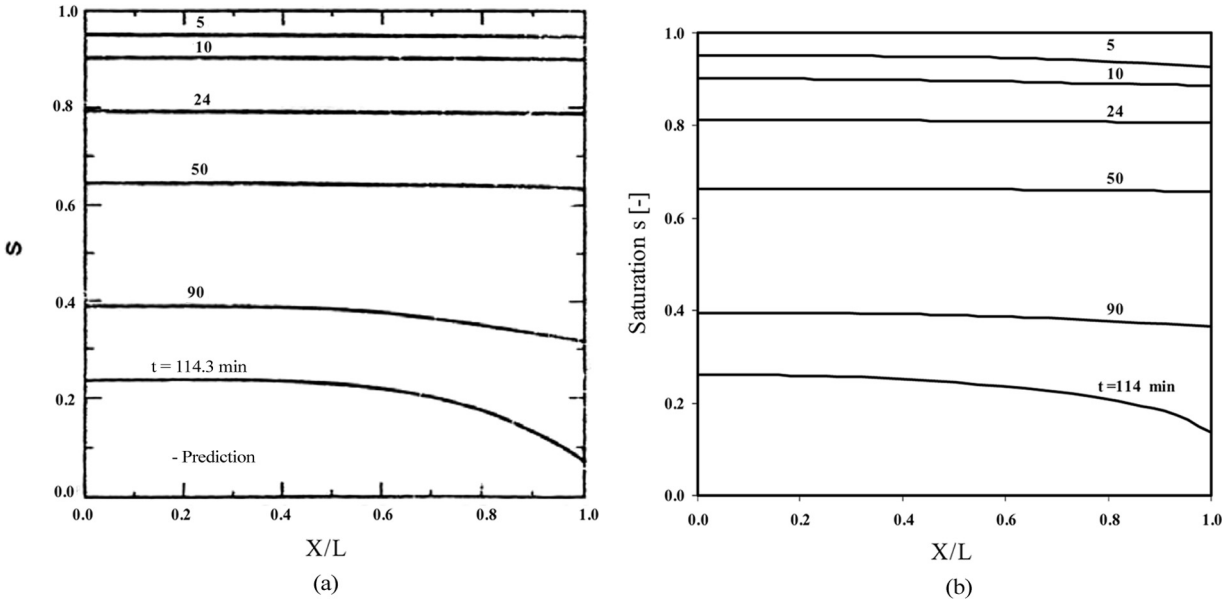

FIG. 3. Saturation profiles with respect to elapsed time. (a) Predicted result from Rogers and Kaviany,[26] (b) predicted result from present study.

actual thickness wall) remains under atmospheric conditions, allowing heat and mass to freely transfer from the both surfaces to the surrounding.

The case of with gravitational force is first conducted. The effect of initial saturation, S_in, of unsaturated porous slab is carried out on three different initial saturation values; 0.1, 0.3, and 0.7. The case of $S\_in = 0.3$ and $S\_in = 0.7$ are examined. The temperature distributions over time are graphically shown in Figs. 4 and 5. When a wall is heated by hot gas flowing over its upper surface, the heat is transferred from the top of wall to the interior. Therefore, the temperature gradient is formed in the wall. It is obvious that, at each period, temperature reaches the highest at the heated surface due to the existence of the hot gas. At the locations away from the hot surface, the temperature decreases and becomes equal to the ambient temperature at the atmospheric boundary. The steep curve near the hot surface indicates a high heat transfer rate. In addition, the overall temperature increases with time.

As shown in Figs. 6 and 7, total pressure distributions at the early stage are in vacuum zone as gaseous are formed and slowly fill in voids. Four hours later, total pressure

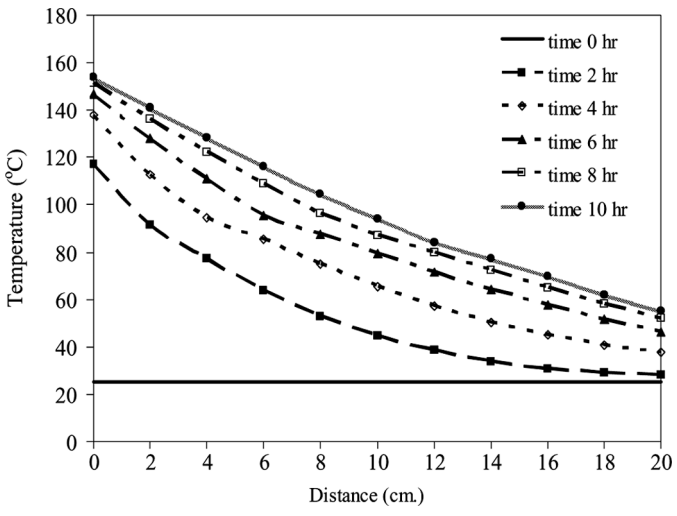

FIG. 4. Temperature distribution as a function of depth and time from the unsaturated porous slab exposed to hot gas in the case with gravitational force ($S\_in = 0.3$).

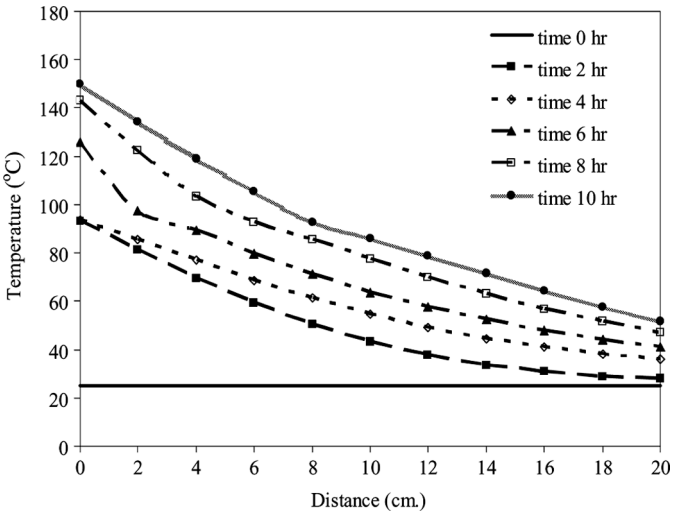

FIG. 5. Temperature distribution as a function of depth and time from the unsaturated porous slab exposed to hot gas in the case with gravitational force ($S\_in = 0.7$).

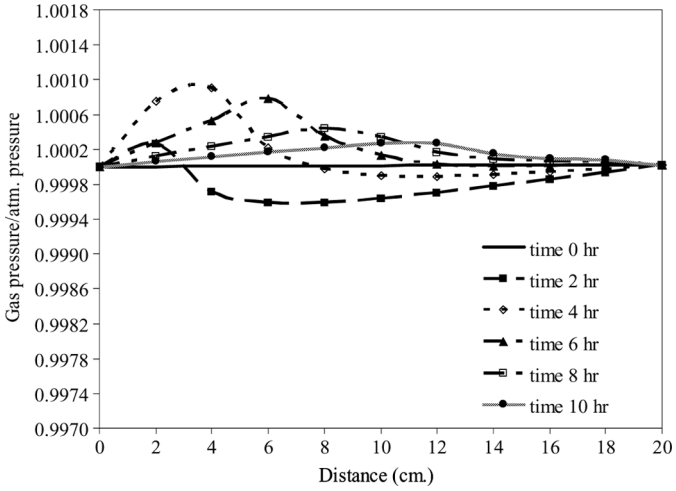

FIG. 6. Pressure distribution as a function of depth and time from the unsaturated porous slab exposed to hot gas in the case with gravitational force ($S\_in = 0.3$).

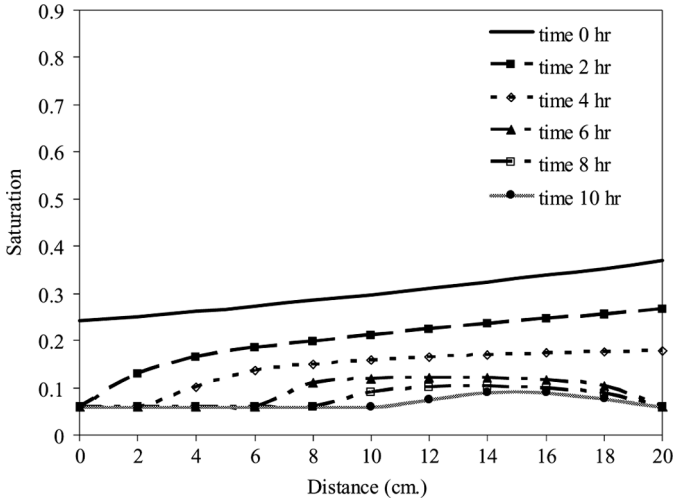

FIG. 8. Saturation distribution as a function of depth and time from the unsaturated porous slab exposed to hot gas in the case with gravitational force ($S\_in = 0.3$).

builds up rapidly near the heated surface. High diffusive vapor flux also contributes to an increase in total pressure. The pressure keeps rising with time. However, total pressure of the colder regions at the beginning period remains in vacuum. High temperature and pressure gradient are generated within the unsaturated porous slab, particularly in the early stage of heating; initiate a pumping effect. As a result, a great amount of liquid is supplied to the surface. The mechanism of moisture transfer is mainly affected by capillary pressure. The saturation distributions shown in Figs. 8 and 9, reduce fast, particularly at the hot surface as resulted from the high liquid extraction rate. Liquid accumulates at the bottom of the unsaturated porous slab at any time due to reflection of the inclined curves. At the wet surface, liquid in the upper zone evaporates with the variation of saturated vapor concentration which corresponds to the temperature gradient.

As heat and mass transport progresses, capillary effects become less pronounced and vapor diffusion takes more effect instead. As a result, there will be less liquid from capillary action than that from evaporation. Therefore, the interior of the wall is divided into two layers by the moving evaporation front and there are liquid water and gas inside the layers. In a place where there is only gas

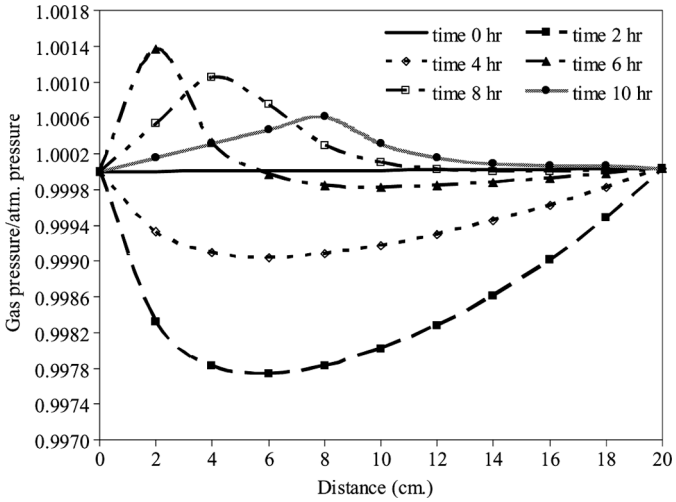

FIG. 7. Pressure distribution as a function of depth and time from the unsaturated porous slab exposed to hot gas in the case with gravitational force ($S\_in = 0.7$).

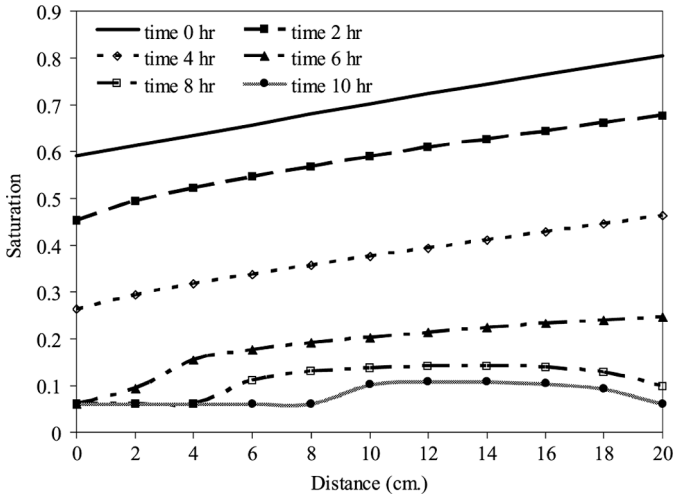

FIG. 9. Saturation distribution as a function of depth and time from the unsaturated porous slab exposed to hot gas in the case with gravitational force ($S\_in = 0.7$).

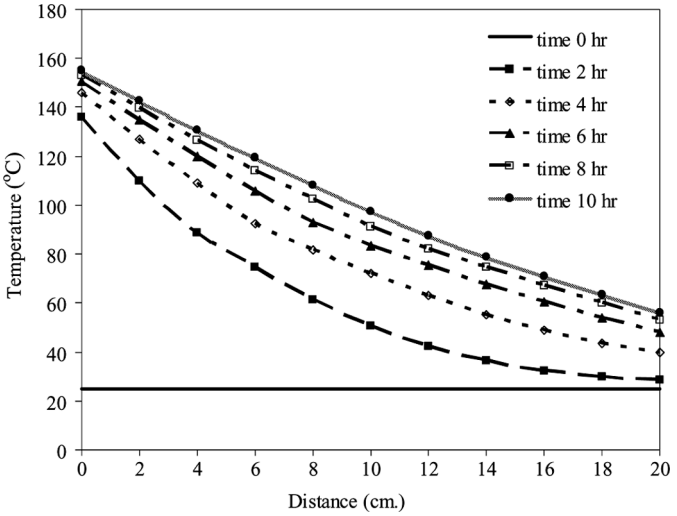

FIG. 10. Temperature distribution as a function of depth and time from the unsaturated porous slab exposed to hot gas in the case with gravitational force ($S\_in = 0.1$).

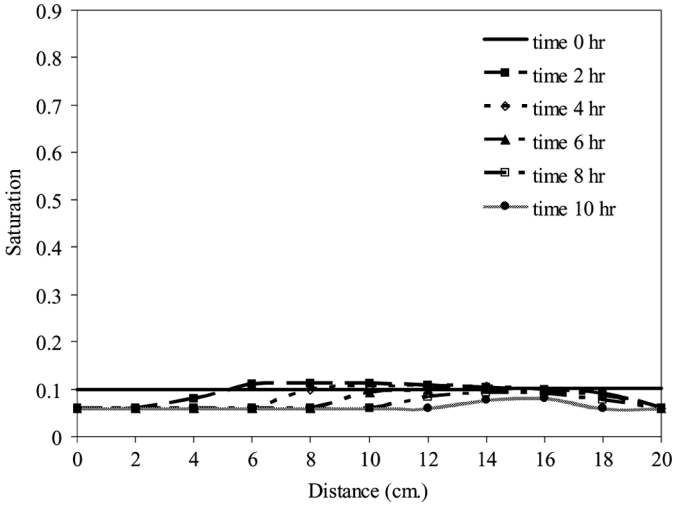

FIG. 12. Saturation distribution as a function of depth and time from the unsaturated porous slab exposed to hot gas in the case with gravitational force ($S\_in = 0.1$).

phase, water vapor is transferred toward the upper or lower surface by the effects of the vapor diffusion, thermo-capillary action, motion, and gravity. Near the hot surface, the value of saturation approaches 0.06,which is the minimum saturation of unsaturated porous slab. This condition is referred to as dry zone condition. After this stage, the amount of liquid inside the wall will not decrease further. Since the formation of a dry layer acts as thermal resistance of the heat transfer from the hot gas, the evaporation rate decreases remarkably compared to that for a wetted surface. This state is generally known as the period of falling rate.[27] The statebefore formation of a dry layer is called the period of constant rate because the evaporation rate is nearly constant. As a result, liquid is accumulated, thereby, causing the total pressure buildup as shown in Figs. 6 and 7. It is also noted that pressure was peak near the boundary of dry zone inside the concrete. This peak corresponds to the buildup pressure from liquid accumulation which is no longer extracted under dry zone condition. The saturation curve ascends from the top to the bottom of heated surface. This phenomenon is mainly caused by the gravitational effect that enhances the downward movement of liquid towards the bottom boundary. It is clear that the gravitational force also influences the

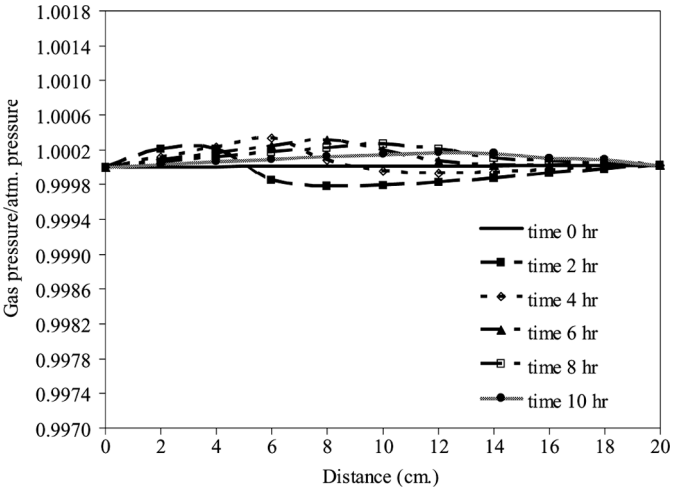

FIG. 11. Pressure distribution as a function of depth and time from the unsaturated porous slab exposed to hot gas in the case with gravitational force ($S\_in = 0.1$).

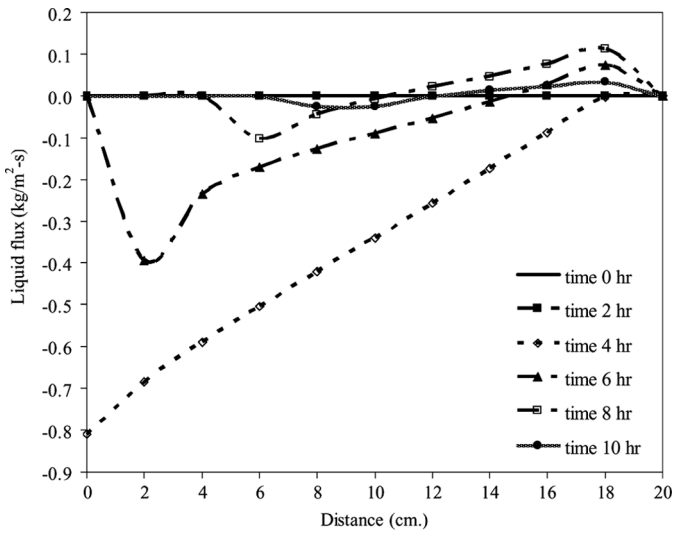

FIG. 13. Liquid flux distribution as a function of depth and time from the unsaturated porous slab exposed to hot gas in the case with gravitational force ($S\_in = 0.7$).

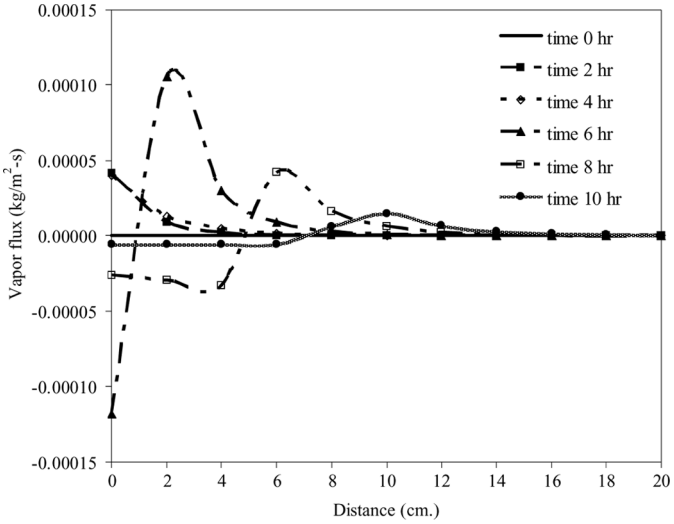

FIG. 14. Vapor flux distribution as a function of depth and time from the unsaturated porous slab exposed to hot gas in the case with gravitational force ($S\_in = 0.7$).

liquid transport behavior. In these two cases ($S\_in = 0.3$ and $S\_in = 0.7$), they give similar trend of distribution. In comparison with the case of $S\_in = 0.3$, the pressure distribution of $S\_in = 0.7$ is considerably higher as resulted from more amount of saturated water filled in pores. Due to larger rate of liquid extraction in which the volume of gas is enlarged for the case of $S\_in = 0.3$, the total pressure distribution takes more vacuum zone.

To learn about effects of saturation, distributions of temperature, total pressure, and saturation at $S\_in = 0.1$ 0.1 are also studied and their results are depicted in

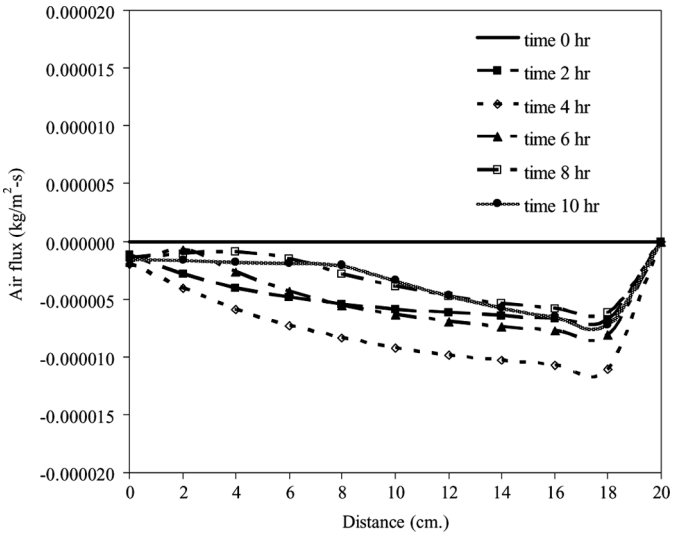

FIG. 15. Air flux distribution as a function of depth and time from the unsaturated porous slab exposed to hot gas in the case with gravitational force ($S\_in = 0.7$).

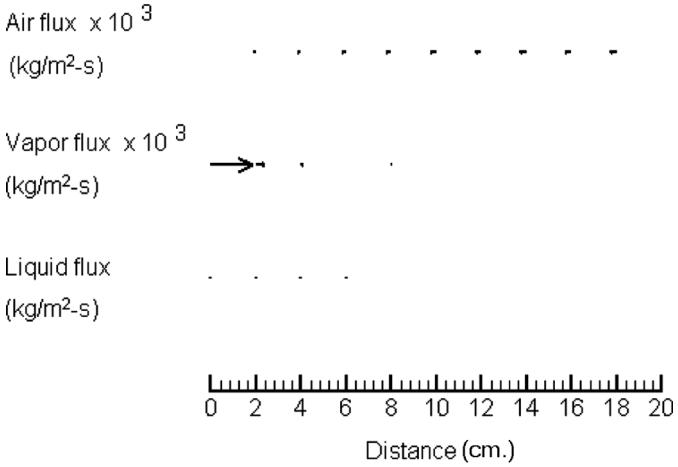

FIG. 16. Fluid movement pattern as a function of depth from the unsaturated porous slab exposed to hot gas at 2 hour in the case with gravitational force ($S\_in = 0.7$).

Figs. 10–12. In the beginning with the presence of dry zone, temperature rises at a faster rate for the small value of the initial saturation. For $S\_in = 0.1$, total pressure and saturation variations are the same as those of 0.3 and 0.7 except for smaller magnitudes since less amount of saturated water is filled in pores. Due to low initial saturation, liquid can easily flow and fill the pores within the medium. Then gas volume is reduced and leads to pressure buildup near the hot wall. The total pressure also peaks near the location where the dry zone ends.

It is important to study the fluid movements in unsaturated porous slab in depth. The liquid flux profiles, the vapor flux profiles and the air flux profiles for the case of $S\_in = 0.7$ at various times are depicted in Figs. 13–15, respectively. It can be seen in Fig. 13 that most of the liquid flows towards the hot surface, where evaporation takes

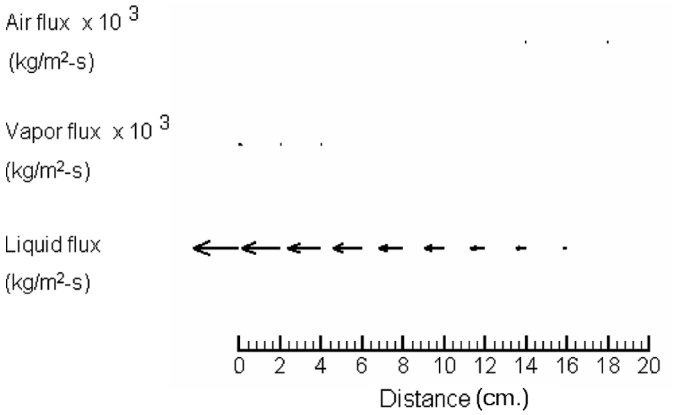

FIG. 17. Fluid movement pattern as a function of depth from the unsaturated porous slab exposed to hot gas at 4 hour in the case with gravitational force ($S\_in = 0.7$).

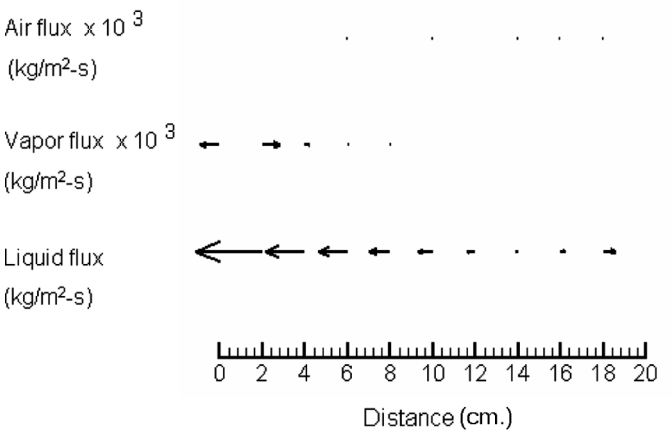

FIG. 18. Fluid movement pattern as a function of depth from the unsaturated porous slab exposed to hot gas at 6 hour in the case with gravitational force ($S\_in = 0.7$).

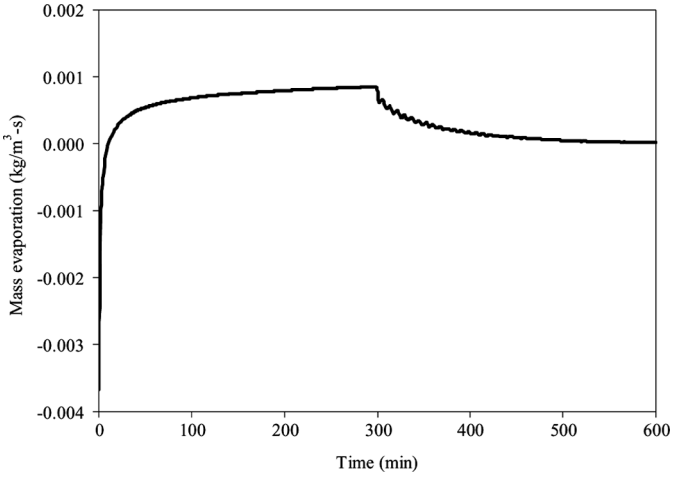

FIG. 20. Mass evaporation rate distribution at the heating surface as a function of time from the unsaturated porous slab exposed to hot gas in the case with gravitational force ($S\_in = 0.7$).

place. Liquid flows in the direction of decreasing saturation, shown earlier in Fig. 9. In the first 2 h, there is no liquid movement due to more amount of saturated water filled in pores. The next 4 h, the liquid flux in large quantities move to the hotter direction; however, these quantities are lessened when the heating period is lengthened. Thus, it is clearly seen in the same figure that after 8 h the liquid flux rarely moves to the hotter direction, especially to the dry zone region. Obviously, a little flux moves to the atmospheric surface during the 8th to 10th hour due to the condensation along the vapor path.

Figure 14 shows the vapor flux distribution at various times. Initially, there is a large amount of vapor flux near the hot surface and the flux moves towards the atmospheric surface. The amount of vapor flux tends to decrease when its direction goes to the atmospheric surface. It can be seen that little vapor flux moves towards the hot surface. From 4 h as the unsaturated porous slab begins to dry, liquid flux then moves up to the evaporation front where the dry zone starts. In the early heating time (before 6 h) while the vapor moves away from the hot surface to the cooler surface, due to thermo-capillary, condensation occurs. From 6 h, at the end of dry zone, the vapor flux becomes to move into two directions towards both sides of the boundary. This is because pores are no longer filled with liquid in the dry zone, allowing the vapor to diffuse to the heated surface.

Figure 15 indicates the air flux distribution. The larger amount of air flux occurs near the atmospheric surface, and moves to the hot surface. It is clear that air flux flows to the hot surface only. However, the flows appear to be an unusual shape. As previously mentioned, after 4 h its

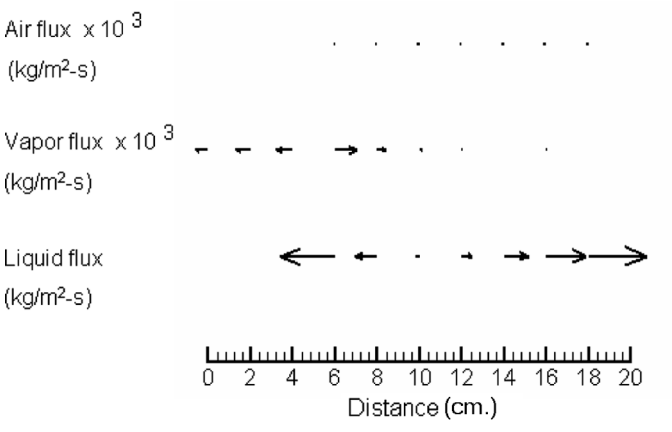

FIG. 19. Fluid movement pattern as a function of depth from the unsaturated porous slab exposed to hot gas at 8 hour in the case with gravitational force ($S\_in = 0.7$).

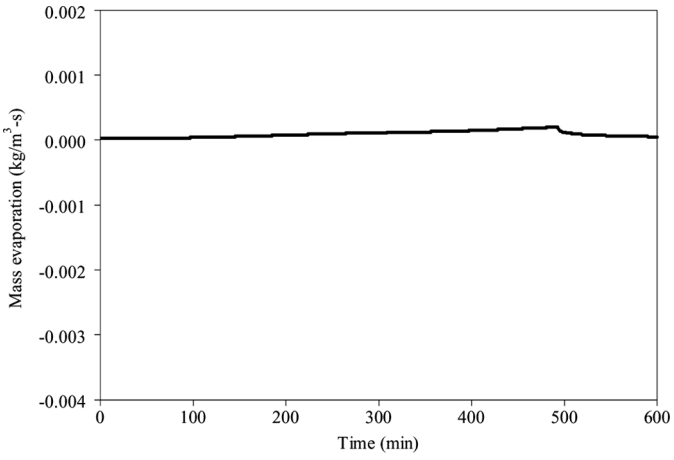

FIG. 21. Mass evaporation rate distribution at the cooling surface as a function of time from the unsaturated porous slab exposed to hot gas in the case with gravitational force ($S\_in = 0.7$).

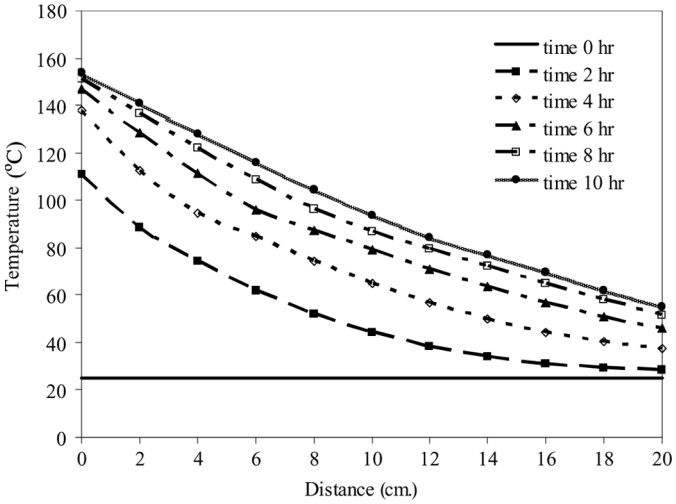

FIG. 22. Temperature distribution as a function of depth and time from the unsaturated porous slab exposed to hot gas in the case without gravitational force ($S\_in = 0.3$).

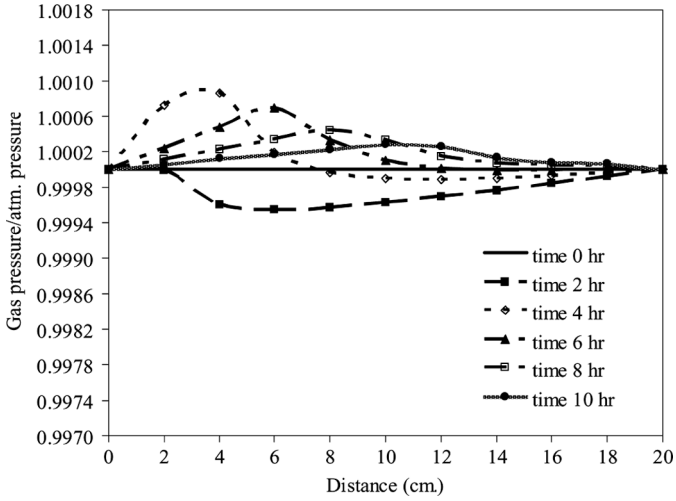

FIG. 24. Pressure distribution as a function of depth and time from the unsaturated porous slab exposed to hot gas in the case without gravitational force ($S\_in = 0.3$).

magnitude decreases due to an increase of void volume thereby slowing down the air supply rate.

Figures 16–19 show the vector profiles in a similar configuration to Figs. 13–15. For the case that $S\_in = 0.7$, 0.7, the fluid movement patterns in the porous slab as a function of depth from the heated side at 2, 4, 6, and 8 h are illustrated in Figs. 16–19, respectively. The vector profile that is presented has an advantage to better clarification of directions and magnitudes. Although there exists transient flow pattern in the beginning, during most of the heating period, water vapor condenses along its path as it flows toward the atmospheric surface. Air also moves in the same direction with liquid water, but with smaller flux, whereas liquid water migrates towards the hot and atmospheric surface with three order of magnitude higher than that of the vapor flux. The vectors plots demonstrate that at the end of heating period (6 and 8 h) liquid and vapor flux moves in two directions. The vapor flux is found larger than air flux since the vapor diffusion is enhanced by convective flow of vapor, whereas air diffusion is retarded by convective air flow.

Figures 20 and 21 show mass evaporation flux density at the heating surface and cooling surface as a function of time for the case of with gravitational force ($S\_in = 0.7$). In Fig. 20, the mass evaporation varies sharply in the early time. Surface evaporation is essentially governed by two

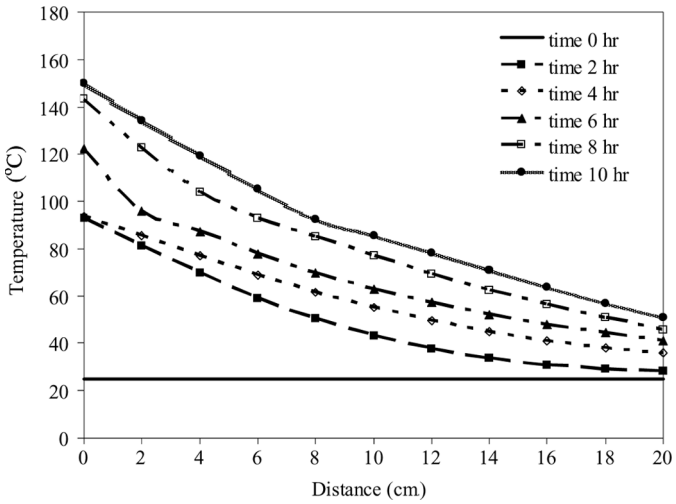

FIG. 23. Temperature distribution as a function of depth and time from the unsaturated porous slab exposed to hot gas in the case without gravitational force ($S\_in = 0.7$).

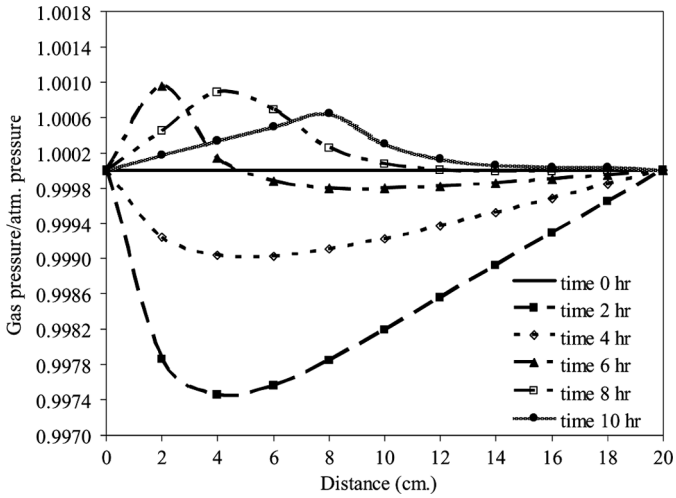

FIG. 25. Pressure distribution as a function of depth and time from the unsaturated porous slab exposed to hot gas in the case without gravitational force ($S\_in = 0.7$).

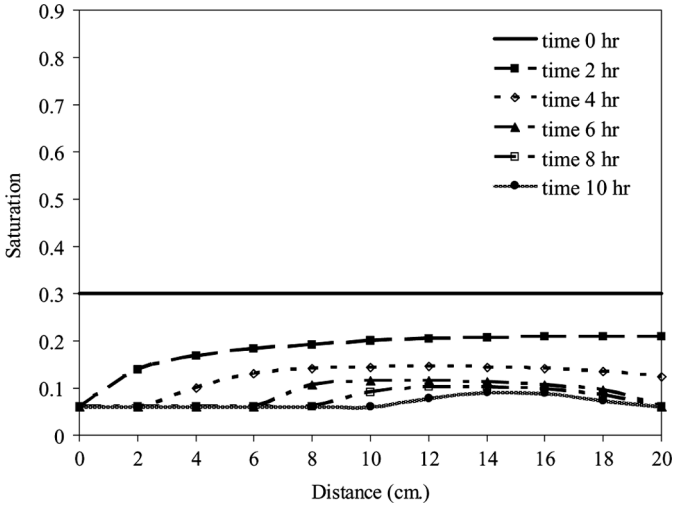

FIG. 26. Saturation distribution as a function of depth and time from the unsaturated porous slab exposed to hot gas in the case without gravitational force ($S\_in = 0.3$).

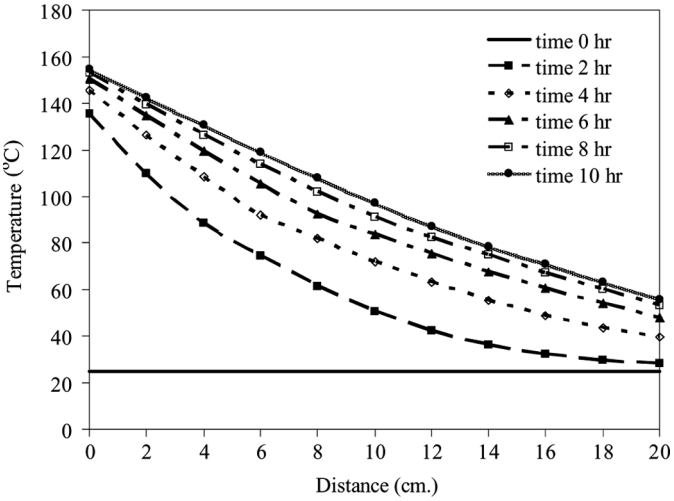

FIG. 28. Temperature distribution as a function of depth and time from the unsaturated porous slab exposed to hot gas in the case without gravitational force ($S\_in = 0.1$).

factors, namely the surface temperature and the fraction of wet surface. In the beginning, fast increase of the evaporation rate is mainly due to the rapid increase to surface temperature, because liquid supply from the interior under the capillary action is sufficient to maintain the surface totally wet. As surface evaporation increases, it reaches a point where the rate of liquid supply to surface become less than the rate of surface evaporation and the surface starts to dry off (fraction of wet surface reduces). Therefore, the increase of evaporation rate is slowed down. In the middle of the heating period when the surface is dry and the increase in temperature is substantially slowed, the evaporation rate decreases rapidly and eventually became nearly constant. In Fig. 21, on the other side of the wall, the corresponding evaporation rate is very small since its surface is exposed to an ambient air which leads to very small driving force.

In what follow, the numerical analysis is also extended to the case that gravitational effect is neglected. Temperature distributions for various S_in of 0.3, 0.7, and 0.1 shown in Figs. 22, 23, and 28 are similar to the case of with gravitational force as presented earlier in Figs. 4, 5, and 10. The pressure distribution is shown in Figs. 24, 25, and 29 for a variety of initial saturations. It is easily seen that the difference of total pressure between the case of with and without gravitational force is very slight. However, based on the saturations depicted in

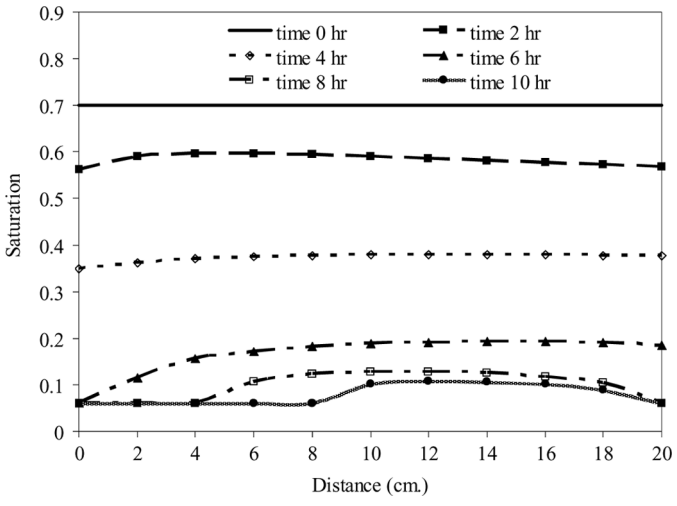

FIG. 27. Saturation distribution as a function of depth and time from the unsaturated porous slab exposed to hot gas in the case without gravitational force ($S\_in = 0.7$).

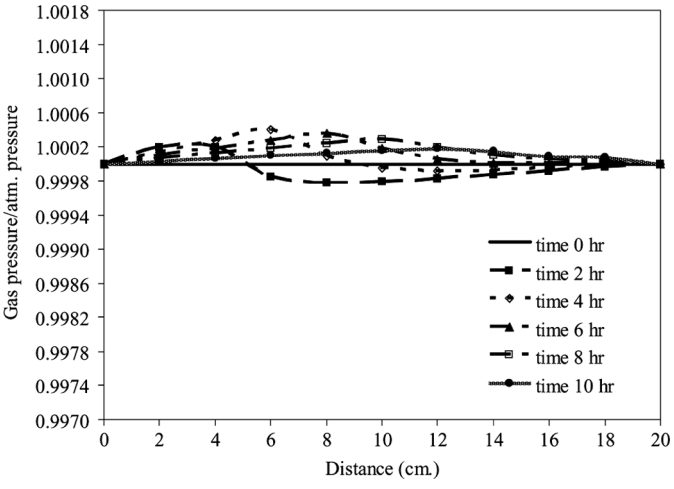

FIG. 29. Pressure distribution as a function of depth and time from the unsaturated porous slab exposed to hot gas in the case without gravitational force ($S\_in = 0.1$).

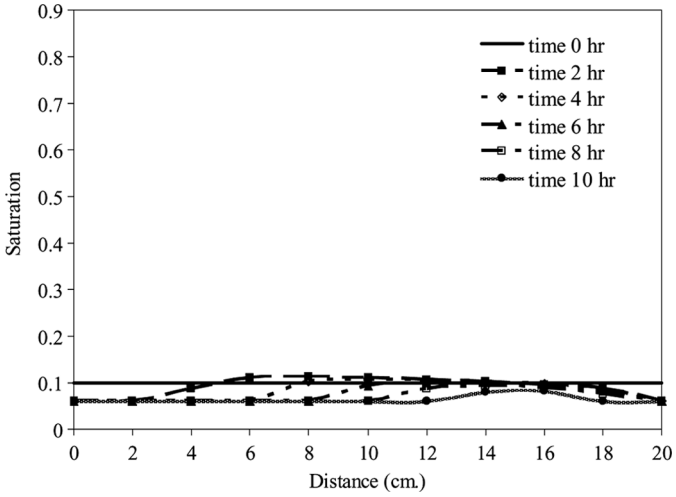

FIG. 30. Saturation distribution as a function of depth and time from the unsaturated porous slab exposed to hot gas in the case without gravitational force ($S\_in = 0.1$).

Figs. 26, 27, and 29, the two cases differ considerably. The case with gravitational effect presents large gradients of saturation in the direction of gravitational force. However, this effect is more pronounced with greater initial saturation.

CONCLUSIONS

The numerical model to describe the coupled heat and mass transfer in unsaturated porous slab exposed to hot gas has been developed. The conditions with and without gravitational force are studied with the application of three different initial saturations. The governing equations are solved using Newton-Raphson method based on a finite volume technique. For all cases of initial saturations, temperature is higher closer to the heated surface due to the hot gas. Large gradients of saturation in the direction of gravitational force appear in the case with gravitational effect that enhances the downward movement of liquid toward the bottom boundary. The pressure is highest near the location where the dry zone ends. The gradient of vapor pressure generates gaseous diffusion towards the surface. In addition, liquid flows in the direction of decreasing saturation. As the unsaturated porous slab begins to dry, liquid flux moves up to the evaporation front in which the dry zone starts. The vapor flux appears to flow into two directions when the dry zone condition is reached at both sides of boundary. The vapor flux is found larger than air flux since the vapor diffusion is enhanced by convective flow of vapor, whereas air diffusion is retarded by convective air flow. The pressure builds up near the interface between wet and dry zone where substantial amount of liquid is accumulated. The unsaturated porous slab temperature as well as total pressure increases with time. This study concludes that under the given conditions, there is a little impact of total pressure to the unsaturated porous slab exposed to hot gas at 170°C.

NOMENCLATURE

C_p	Specific heat capacity (J/kg K)
D_m	Effective molecular mass diffusion (m^2/s)
D_o	Binary mass diffusion in plain media (m^2/s)
g	Gravitational constant (m/s^2)
h_c	Heat transfer coefficient (W/m^2 K)
h_m	Mass transfer coefficient (W/m^2 K)
h_v	Specific heat of vaporization (J/kg)
K	Permeability (m^2)
M	Molecular weight of the gaseous mixture (kg/kmol)
$\dot{n}$	Phase change term (kg/m^3 s)
p	Internal total pressure (Pa)
R	Universal gas constant (J/kmol K)
s	Water saturation
s	Saturation
T	Absolute temperature (K)
t	Time (s)
u	Velocity (m/s)

Greek Letters

ε	Emissivity
λ	Effective thermal conductivity (W/m K)
μ	Dynamic viscosity (kg/m s)
ρ	Density (kg/m^3)
σ	Stefan-Boltzman constant (W/m^2 K^4)
ϕ	Porosity

Subscripts

a	Air
atm	Atmospheric pressure
c	Capillary
e	Effective
g	Gas
l	Liquid water
o	Initial condition
p	Particle
r	Relative
v	Water vapor
∞	Free stream

ACKNOWLEDGEMENT

The authors gratefully acknowledge Thailand Research Fund (TRF) for supporting this research project.

REFERENCES

1. Kaviany, M. *Principle of Heat Transfer in Porous Media*; Springer: New York, 1991.
2. Nield, D.A.; Bejan, A. *Convective in Porous Media*; Springer-Verlag: New York, 1991.
3. Whitaker, S. Theory of drying in porous media. Advances in Heat Transfer **1997**, *13*, 119–203.

4. Patankar, S.V. *Numerical Heat Transfer and Fluid Flow*; McGraw-Hill: New York, 1980.
5. Boukadida, N.; Ben Nasrallah, S.; Perre, P. Mechanism of heat and mass transfer during convective drying of porous media under different drying conditions. Drying Technology **2000**, *18*, 1367–1388.
6. Perre, P.; Turner, I.W. A3D version of TransPore, A comprehensive heat and mass transfer computational model for simulating the drying of porous media. International Journal of Heat and Mass Transfer **1999**, *24*, 4501.
7. Ratanadecho, P.; Aoki, K.; Akahori, M. The characteristics of microwave melting of frozen packed beds using a rectangular waveguide. IEEE Transactions on Microwave Theory and Techniques **2002**, *50* (6), 1495–1502.
8. Ratanadecho, P.; Aoki, K.; Akahori, M. Experimental and numerical study of microwave drying in unsaturated porous material. International Communications in Heat and Mass Transfer **2001**, *28* (5), 605–616.
9. Ratanadecho, P.; Aoki, K.; Akahori, M. Theoretical and experimental study of heat and mass transfer mechanism during convective drying of multi-layered packed bed (effects of particle sizes and layered structure). Journal of Heat Transfer **2002**, *124*, 151–161.
10. Perre, P.; Moser, M.; Martin, M. Advances in transport phenomena during convective drying with superheated steam. International Journal of Heat and Mass Transfer **1993**, *36* (11), 2725–2746.
11. Ben Nasrallah, S.; Perre, P. Detailed study of a model of heat and mass transfer during convective drying of porous media. International Journal of Heat and Mass Transfer **1988**, *31* (5), 957–967.
12. Chen, P.; David Pei, C.T. A mathematical model of drying processes. International Journal of Heat and Mass Transfer **1989**, *32* (2), 297–310.
13. Wei, C.K.; Davis, E.; Davis, A.; John Gordon, Heat and mass transfer in water-laden sandstone: Convective heating. AICHE Journal **1985**, *31* (8), 1338–1348.
14. Boukadida, N.; Ben Nasrallah, S. Two dimensional heat and mass transfer during convective drying of porous media. Drying Technology **1995**, *13* (3), 661–694.
15. Turner, I.W.; Jolly, P.G. Combined microwave and convective drying of a porous material. Drying Technology **1991**, *9* (5), 1209–1269.
16. Huang, C.L.D.; Siang, H.; Best, C.H. Heat and transfer in concrete slabs. International Journal of Heat and Mass Transfer **1979**, *22*, 252–266.
17. Huang, C.L.D. Multi-phase moisture transfer in porous media subject to temperature gradient. International Journal of Heat and Mass Transfer **1979**, *22*, 1295–1307.
18. Huang, C.L.D.; Gamal, N.; Fenton, D.L. Responses of concrete walls to fire. International Journal of Heat and Mass Transfer **1991**, *34* (3), 649–661.
19. Gong, Z.X.; Song, B.; Mujumdar, A.S. Numerical simulation of drying of refractory concrete. Drying Technology **1991**, *9* (2), 479–500.
20. Gong, Z.X.; Mujumdar, A.S. A model for kiln-drying of refractory concrete. Drying Technology **1993**, *11* (7), 1617–1639.
21. Gong, Z.X.; Mujumdar, A.S. A Two-dimensional finite element model for kiln-drying of refractory concrete. Drying Technology **1995**, *13* (3), 585–606.
22. Gong, Z.X.; Mujumdar, A.S. The influence of an impermeable surface on pore steam pressure during drying of refractory concrete slabs. International Journal of Heat and Mass Transfer **1995**, *38* (7), 1297–1303.
23. Gong, Z.X.; Mujumdar, A.S. Development of drying schedules for one-side heating drying of refractory concrete slabs based on a finite element model. Journal of the American Ceramic Society **1996**, *79* (6), 1649–1658.
24. Pakdee, W.; Rattanadecho, P. Unsteady effects on natural convective heat transfer through porous media in cavity due to top surface partial convection. Applied Thermal Engineering **2006**, *26*, 2316–2326.
25. Gawin, D.; Pesavento, F.; Schrefler, B.A. Towards prediction of the thermal spalling risk through a multi-phase porous media model of concrete. Computer Methods in Applied Mechanics and Engineering **2006**, *195*, 5707–5729.
26. Rogers, J.A.; Kaviany, M. Funicular and evaporative-front regimes in convective drying of granular beds. International Journal of Heat and Mass Transfer **1992**, *35* (2), 469–480.
27. Van Brakel, J.; Heertjes, P.M. On the period of constant drying. Proceedings of the 1st International Symposium on Drying; **1968**, Montreal, Canada, 70–75.